ACS APPLIED ENERGY MATERIALS

www.acsaem.org Article

Utilization of Li-Rich Phases in Aluminum Anodes for Improved Cycling Performance through Strategic Thermal Control

Tianye Zheng,* Jia Zhang, Wei Jin, and Steven T. Boles*

Cite This: https://doi.org/10.1021/acsaem.2c03673 Read Online

ACCESS | Metrics & More | Article Recommendations | Supporting Information

ABSTRACT: Lithium-ion batteries with aluminum anodes had appeared to resolve critical dendrite issues of lithium metal cells in the 1970s. However, the poor cycling performance attributed to aluminum anodes would lead to their obsolescence. In this work, we demonstrate how strategic thermal control in cycling aluminum anodes circumvents the problematic α/β phase transformations that yield poor cycling life. Instead, electrochemical formation of the Li_3Al_2 and $Li_{2-x}Al$ phases necessitates temperatures slightly above ambient, as the Li_3Al_2 and $Li_{2-x}Al$ phases are key enablers for high capacity and stable cycling. While delivering a competitive capacity level (ca. 1 Ah kg^{-1}-Al), cycling among those higher-order phases is found to be significantly improved, from several cycles to 100 cycles with ca. 67% capacity retention. Importantly, because modern battery charging is likely to occur above room temperature due to ohmic heating, the thermal conditions explored here are expected to be realized in a variety of applications. Furthermore, we show that elevated temperature is not necessary for aluminum anode delithiation, thus creating additional synergies with many practical scenarios.

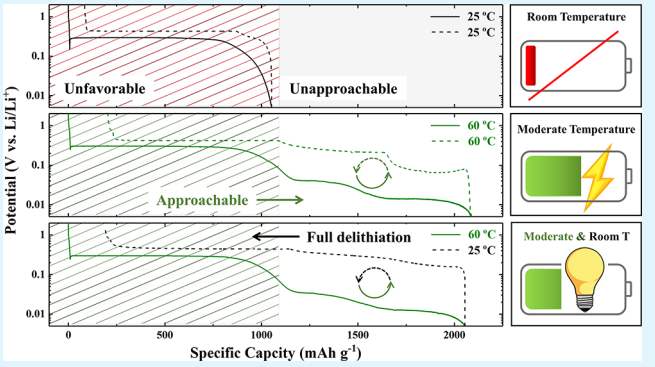

KEYWORDS: *lithium-ion battery, aluminum anode, moderate temperatures, phase transformations, Li-rich phases, asymmetrical thermal cycling*

INTRODUCTION

Lithium-ion batteries (LIBs) are emerging as one of the most promising energy storage devices, playing vital roles in the fields of manufacturing, e-mobility, and renewable energy industry. While most people became acquainted with LIBs in the early 1990s when SONY successfully commercialized cells with carbon-based anodes and brought them to market,[1] from a scientific perspective, the concept of LIBs is considerably older and originates with the discovery of Na-β-alumina and the first generation of Li-metal batteries in the late 1960s.[2] Regardless of the cathode material, elemental Li was the primary anode in the first-generation Li-based cells until the severity of the problems caused by the formation of dendrites during Li plating was recognized, as short circuits lead to serious safety hazards.[3]

An aluminum (Al) alloy anode was then introduced at that very moment to resolve critical safety issues. It was found by Exxon that a LiAl alloy anode could effectively suppress the growth of Li dendrites on its surface.[4] This cell design was the predecessor of LIB where both the anode and cathode serve as Li hosts with no metallic Li present. However, the reversibility of LiAl alloy anodes would prove to be unsatisfactory, usually losing most of its capacity after a dozen of cycles if the full capacity of the cell was to be utilized. Attempts had been made to understand the mechanisms behind the fast capacity decay of LiAl alloy[5−18] until Yoshino's team put together the carbon anode and the $LiCoO_2$ cathode in 1985 and officially named it a lithium-ion battery.[19] Since then, the research focus on anodes had been shifted from LiAl alloy to a carbon-based one (graphite) and eventually triggered the successful commercialization and popularization of LIBs. Entering the 21st century, people started looking for anode materials with higher specific capacities to fulfill larger-scale applications, such as electric vehicles (EVs) and renewable energy storage. Silicon and tin have been extensively studied due to their high theoretical capacity figures, while LiAl alloy seems to be nearly forgotten by academia presumably because the reliability and stability seem insurmountable. However, in recent years, several new studies have revisited the topic to investigate LiAl alloy as the anode for LIB applications.[20−27] While it is known that the capacity originates from the phase transformations between the α phase Al (face-centered cubic) and the β phase LiAl (NaTl, B32-type) at room temperature (RT), a well-adopted capacity

Received: November 15, 2022
Accepted: January 24, 2023
Published: January 31, 2023

value of ca. 1 Ah kg^{-1} is routinely cited in the literature. However, according to the Li−Al binary phase diagram, there exist multiple Li−Al phases beyond the β-LiAl, such as Li_3Al_2, $Li_{2-x}Al$, and Li_9Al_4. Unlike β-LiAl, which is well studied in recent years, the higher-order phases are seldom reported as they are believed to be only approachable at elevated temperatures, although these phases give significantly higher capacities.[28,29]

In reviewing major applications of LIBs, such as EVs and stationary energy storage, sophisticated cooling systems are usually implemented to dissipate the waste heat generated during charging and to reach minimum temperatures to avoid lithium plating. For instance, Tesla EVs allow the battery pack to heat up to 55 °C before activating the built-in active cooling system because a faster ion diffusion (i.e., faster charging) can be facilitated by higher temperatures. Therefore, operating LIBs at slightly elevated temperatures is acceptable or even preferred, but naturally is limited to moderate temperatures, e.g., not above 60 °C (Panasonic),[30] to ensure safe and reliable operations. In this work, we aim to demonstrate how moderate temperature control of Al anodes (e.g., 60 °C) can lead to exciting new prospects for one of the oldest established lithium-ion battery anodes. While Ghavidel et al. reported that both Li_3Al_2 and $Li_{2-x}Al$ can readily form electrochemically at a temperature as low as 35 °C,[29] our studies shed light on the cyclability of these phases and practical strategies for their utilization.

EXPERIMENTAL SECTION

Electrode Fabrication. Al thin films are sputtered onto Cu foil current collectors using physical vapor deposition (PVD) equipment (MAT 400, Germany). A 12-in. high-purity Al target (99.999%) was used to carry out the thin film deposition for 40 min at 1000 W incident power with 50 sccm Ar flow as the background. The temperature of the sputtering chamber was set at 100 °C. The sputtered Al films are estimated to have a thickness of ca. 1.8 μm based on both the precalibrated deposition rate. The estimated thickness was also examined by the electrochemical lithiation, assuming conversion to the 1:1 LiAl alloy, thereby yielding ∼0.48 mAh cm^{-2}.

Material Characterization. High-resolution X-ray diffraction (XRD; Rigaku SmartLab, Japan) is the main technique that was performed to explore the phase structures of fully lithiated Al foils (20 μm thick; cathode current collectors) on behalf of the above-mentioned Al films to achieve stronger diffraction peaks of LiAl alloys. The scan step was 5°/min in the 2θ range of 20°−50° with the 45 kV maximum voltage and 200 mA maximum current.

Electrochemical Characterization. The 2025-type coin cells were assembled with Al thin films/foils as the working electrode and Li foils as the counter electrode. A glass fiber sheet (Whatman) and 1 M $LiPF_6$ in EC:PC 1:1 vol % were used as the separator and the electrolyte, respectively. All electrochemical tests were performed using a VMP potentiostat (Biologic Technologies, France). Cyclic voltammetry (CV) and galvanostatic charge−discharge (GCD) were performed both at room and moderate temperatures (25−60 °C). The moderate temperatures were achieved using a basic thermal chamber.

RESULTS AND DISCUSSION

Material and Electrochemical Characterizations. X-ray diffraction (XRD) is used to probe the Li−Al phases that are formed upon electrochemical lithiation at 60 °C and room temperature (25 °C) with 20 μm thick Al foils. The diffractograms presented in Figure 1a indicate that the $Li_{2-x}Al$ phase (JCPDS card 1-79-8685) is the major crystalline

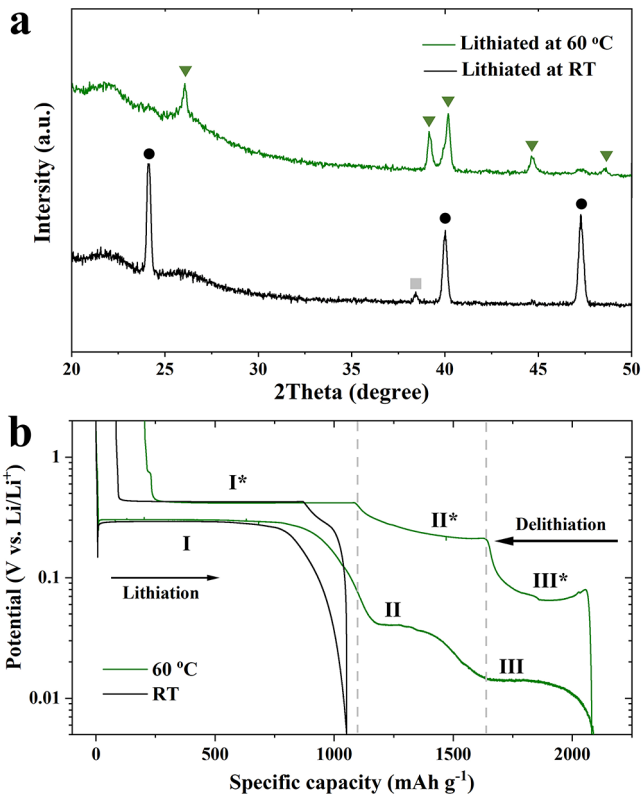

Figure 1. (a) X-ray diffractograms obtained from fully lithiated Al foil electrodes (20 μm thick) at 60 °C and RT (room temperature); gray square: α-Al; black circle: β-LiAl; green triangle: $Li_{2-x}Al$); the dense foil is used for achieving clear diffraction peaks while the diffractograms of lithiated Al thin films are provided in the Supporting Information. (b) Galvanostatic charge−discharge (GCD) profile of Al thin film electrodes obtained at 60 °C and RT. The (de)lithiation current is set at 12 μA cm^{-2} with the lower and the upper potential limits of 0.005 and 1.5 V vs Li/Li^+, respectively.

product for the Al foil that is fully lithiated at 60 °C, while only β-LiAl peaks (JCPDS card 03-1215) together with a weak α-Al peak are observed for the room temperature sample. On the basis of our knowledge, the $Li_{2-x}Al$ phase was first identified not long ago in 2010[28] and thus is absent in prior phase diagrams, e.g., in 1982[31] and 1986.[32] As for the highest lithiated phase Li_9Al_4, it is suggested to be only electrochemically approachable at temperatures beyond 100 °C.[29] The in-depth structural analyses, which are beyond the scope of this work, can be found in a comprehensive study that has investigated these phases using *ex situ* XRD techniques.[29]

Figure 1b shows the galvanostatic charge−discharge (GCD) profile of an Al thin film electrode that operates in a half-cell configuration at 60 °C, while the one obtained at room temperature is also given for comparison. The cyclic voltammograms are also provided in Figure S1. The GCD profile exhibits three distinct regions during lithiation, two of which refer to the formation of the higher order phases, Li_3Al_2 (**II**, ∼0.04 V vs Li/Li^+) and $Li_{2-x}Al$ (**III**, 0.014 V vs Li/Li^+) phase, in addition to the well-known β-LiAl (**I**, ∼0.3 V vs Li/Li^+). The corresponding delithiation plateaus are ∼0.09, ∼0.22, and ∼0.42 V vs Li/Li^+, for the regions **III***, **II***, and **I***, respectively. These two extra plateaus at 60 °C also contribute to a significantly higher capacity, roughly double that of β-LiAl, giving ca. 2 Ah kg^{-1}. To examine the feasibility of utilizing these newly formed phases in real applications, a

https://doi.org/10.1021/acsaem.2c03673
ACS Appl. Energy Mater. XXXX, XXX, XXX−XXX

full cell is assembled by pairing an Al thin film with a prelithiation LTO, i.e., $Li_7Ti_5O_{12}$, and cycled at 60 °C. The GCD profile of the full cell is provided in Figure S2, from which extra capacity contributed by the higher order phases is observed, agreeing with that of the half-cell (Figure 1b).

Moreover, some electrochemical features should be discussed here. First, the irreversible capacity of the initial cycle is larger for the cell at 60 °C (204 mAh g^{-1}) than that for the cell at room temperature (85 mAh g^{-1}). A dummy cell (i.e., Cu foil vs Li metal) is assembled and operates at 60 °C, which delivers a capacity of 28 mAh g^{-1} if normalizing to the Al mass of the regular half cells. Still, the mismatch is about 91 mAh g^{-1} after deducting the capacity calculated from the dummy cell. To better understand the origin of this irreversible capacity, one can notice that the reversibility between β-LiAl and $Li_{2-x}Al$ seems to be ideal, while a poor charge efficiency is observed (and expected) when the β phase is transformed back to the α phase. Therefore, two half-cells are assembled to verify how the reversibility between α and β can be affected by temperatures. One is cycled at 60 °C, and the other is cycled at room temperature. Figure S3 demonstrates that the first-cycle charge efficiency is ca. 87.4 ± 0.2% (131 ± 2 mAh g^{-1} irreversible capacity) for the former and ca. 91.0 ± 0.7% (88 ± 7 mAh g^{-1} irreversible capacity) for the latter (errors come from the control experiments). However, these irreversible capacities of the second cycle are comparable at both temperatures, indicating that the difference in the first-cycle charge efficiency might be a result of the SEI formation (only pronounced during the initial cycle). It should be noted that the cutoff voltage is set at 0.1 V vs Li/Li^+ for a fair comparison, above which the β-LiAl is expected to be the only lithiated phase at the two temperatures. The results here generally support that the higher irreversible capacity at 60 °C in Figure 1a largely comes from the α/β phase transformations (especially when the lower cutoff voltage is considered) rather than from the $Li_{2-x}/Li_3Al_2/\beta$-LiAl ones.

Cycling Performance of β-LiAl/Li_3Al_2/$Li_{2-x}Al$. Although both $\alpha \rightarrow \beta$ and $\beta \rightarrow \alpha$ phase transformations are known to be accompanied by significant volume changes, the latter is generally considered to be responsible for the capacity fading of Al anodes at room temperature. A series of *operando* light microscopy studies have visualized various irreversible degradation mechanisms during phase transformations, including crack formation, pulverization, and formation of nanopores.[33−35] With a ca. 95% difference in lattice volume between the two phases, a nominal compressive stress of ca. 500 MPa may be generated in the vicinity of the transformed region.[35] Like most alloy anode materials, these problems are intrinsically coupled to the host element/matrix and thus are challenging to resolve. Nevertheless, deliberate strategies to circumvent the huge mechanical stress[36] or restrict the β to α phase transformation[37] hold promise for enabling room temperature Al anodes for LIBs. For example, Li et al. managed to confine the lithiation direction of Al foil anodes and thus largely circumvent the mechanical strain caused by the volume expansion. As a result, the anode cyclability (i.e., the reversibility of α/β phase transformations) is markedly improved.[36]

In this work, on the other hand, an alternative pathway of utilizing Li-rich phases in Al anodes is proposed, in addition to the strategies discussed before. All the possible issues regarding the α/β phase transformations can be completely excluded by controlling the cutoff potentials and by slightly increasing the temperature. If cycling can be restricted between the β-LiAl and higher order phases (e.g., $Li_{2-x}Al$), different cycling behavior and degradation are to be expected. Indeed, as illustrated in Figure 2a, an Al thin film is lithiated at 60 °C to

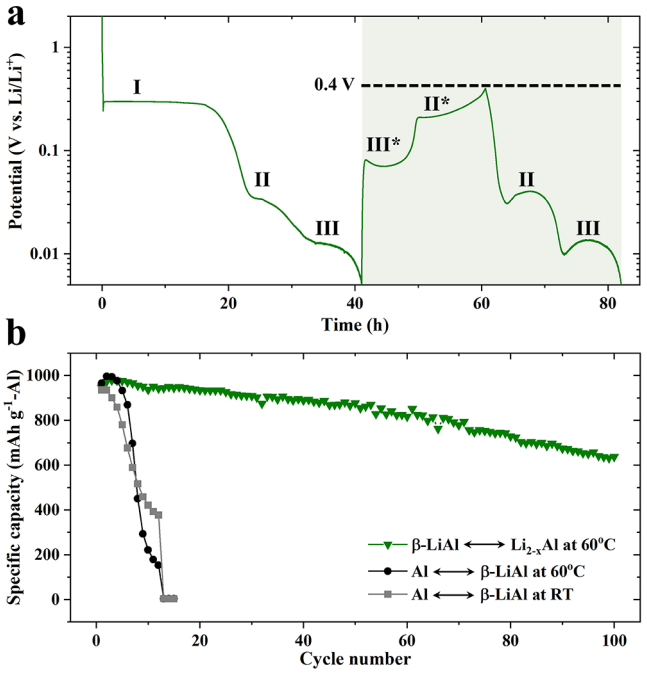

Figure 2. (a) An alternative of galvanostatic cycling that utilizes the capacity contributed by β-LiAl/Li_3Al_2/$Li_{2-x}Al$ phase transformations (α/β phase transformations are prohibited). (b) Cycling performance of the β-LiAl/Li_3Al_2/$Li_{2-x}Al$ phase transformations, i.e., between **III*/II*** and **II/III** in (a), which is compared with the ones of the α/β phase transformations.

0.005 V vs Li/Li^+, and then it is partly delithiated to 0.4 V vs Li/Li^+ at 12 μA cm^{-2} (~C/40 normalized to the capacity of β-LiAl). This 0.4 V delithiation cutoff voltage prevents the formation of α-Al, although the β-LiAl phase is likely at its Li-poor state. Subsequently, the electrode is cycled between 0.4 and 0.005 V vs Li/Li^+ (between **III*/II*** and **II/III**; shaded area in Figure 2a); i.e., the β-to-α phase transformation is intentionally prohibited. Figure 2b reveals that the electrode under such conditions exhibits a significantly longer cycling life as compared to the ones that undergo α/β phase transformations. The specific capacity contributed by the β-LiAl/Li_3Al_2/$Li_{2-x}Al$ lithiation sequence is ca. 950 mAh g^{-1} normalized to Al and clearly with promising reversibility, retaining a ca. 67% (640 mAh g^{-1}-Al) of its first delithiation capacity after 100 cycles. On the other hand, regardless of temperature, the capacity of the control cells which were restricted to α/β phase transformations is completely gone for a dozen cycles, consistent with previous reports.[20,21]

While it is not the intention of the presented cycling performance (Figure 2b) to compete with other anode candidates, it does raise a novel "bypass" for utilizing Al anodes that are cheap, capable of scaled production, and environmentally friendly (at least compared to the state-of-the-art). Although enough evidence can be found from the community that Al is hardly a reliable anode candidate for LIB application, those commonly held perceptions are restricted to the α/β phase transformations because most studies are done at room temperature. In short, the better cycling performance

https://doi.org/10.1021/acsaem.2c03673
ACS Appl. Energy Mater. XXXX, XXX, XXX−XXX

Table 1. Structural Information of Multiple Li−Al Intermetallic Compounds That Can Be Formed Electrochemically at Moderate Temperatures[a]

		lattice information				
phase	crystal	a (Å)	b (Å)	c (Å)	γ (deg)	no. of atoms per unit cell
Al	cubic, face-centered	4.041	4.041	4.041	90	4
β-LiAl	cubic, B32-type	6.348	6.348	6.348	90	8
β-LiAl[8] [b]	cubic, B32-type	6.375[b]	6.375[b]	6.375[b]	90	8
Li_3Al_2	trigonal	4.446	4.446	14.073	120	15
$Li_{2-x}Al$	orthorhombic	4.592	9.596	4.448	90	12
$Li_{2-x}Al$[28] [b]	orthorhombic	4.658[b]	9.767[b]	4.490[b]	90	12

[a]The values are calculated using the minima hopping method (MHM) presented in one study.[40] [b]The data were obtained experimentally.

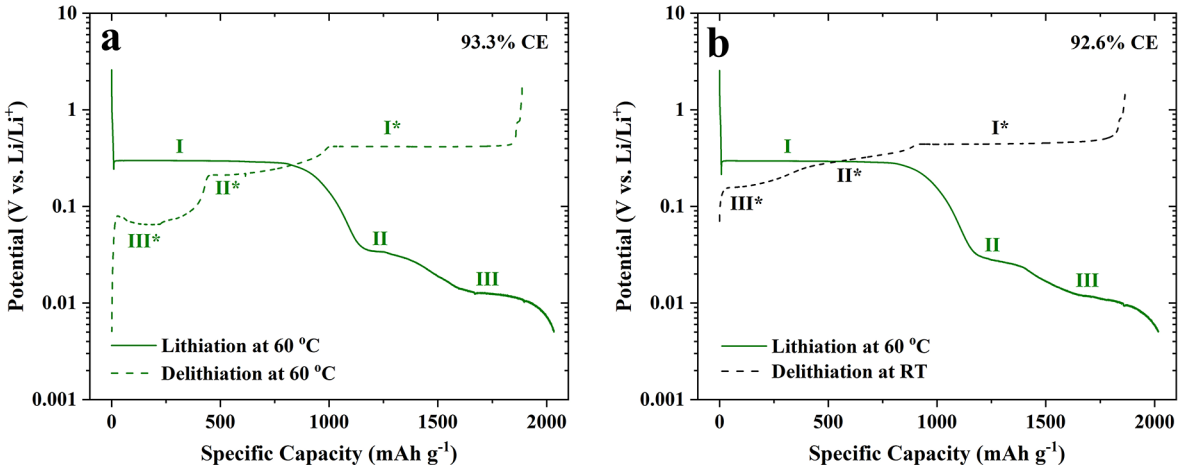

Figure 3. Galvanostatic profiles of the Al thin film electrodes that are lithiated at 60 °C and delithiated at (a) 60 °C and (b) at RT. The quantitative data of the capacities contributed by the lithiation−delithiation are provided in Figure S4.

benefits from the circumvention of the problematic α/β phase transformations, and thus the β-LiAl/Li_3Al_2/$Li_{2-x}Al$ lithiation series merits more consideration and investigation.

The significantly different cycling performances between the α/β phase transformations and the β-LiAl/Li_3Al_2/$Li_{2-x}Al$ ones may partly be explained by the material chemistries and physical properties. Previous Al anode studies rarely discuss the structural information regarding Li-rich phases (except for the work done by Ghavidel et al.[29]) and are thus provided in Table 1. Although the volume difference between the β-LiAl and $Li_{2-x}Al$ is calculated to be ca. 102% (105%*), the Li_3Al_2 phase may act as a buffer between the two phases because the lattice volume of Li_3Al_2 is calculated to be ca. 47% (46%*) larger than that of β-LiAl and ca. 54% (57%*) smaller than that of $Li_{2-x}Al$. As a result, the mechanical strain at the β-LiAl/Li_3Al_2 or the Li_3Al_2/$Li_{2-x}Al$ phase boundary should not be as substantial as that at the α/β one, partly supporting the better reversibility of β-LiAl/Li_3Al_2/$Li_{2-x}Al$ phase transformations.

Additionally, the interatomic (i.e., Al−Al distance) might also play a role in explaining the improved cycling performance when the electrode is limited to β-LiAl/Li_3Al_2/$Li_{2-x}Al$ phases, as presented in Figure 2b. The difference in Al−Al interatomic distance between β-LiAl and $Li_{2-x}Al$ is merely 0.103 Å (~2%), which may be readily accommodated through stretching, distortion, and bond re-forming. By comparison, the Al−Al distance changes dramatically (0.448 Å difference; ~11%) when β-LiAl is forming at the expense of α-Al, necessitating significant atomic rearrangement with each successive half-cycle. With the face-centered cubic (fcc) structure of α-Al, the distance between the Al atoms at vertices on the ⟨001⟩ plane is ~4.041 Å, which is increased to ~4.592 Å once the final lithiated phase at the given temperature, $Li_{2-x}Al$ (orthorhombic) is formed. Considering the intermediate phase of β-LiAl that exists between these two extremes, its Al−Al distance on the same plane is ~4.489 Å (because Al atoms sit on the edge of the unit cell instead of vertices, although the β-LiAl lattice constant is ~6.375 Å).

The mechanical brittleness of β-LiAl[38] is also reported to be responsible for the poor cycling performance of Al-based anodes because some observations support this brittleness, such as cracks of Al films,[23] pulverization of Al wires,[39] and material falloff of Al foils.[37] It is reported elsewhere that the stiffness of Li−Al alloy does not deteriorate when the Li content is beyond 25%, which is determined by the ratio of the bulk over the shear modulus (B/G) of different phases. The soft Al (fcc) and Li (bcc) have B/G ratios of 2.6 and 2.3, while β-LiAl, Li_3Al_2, and $Li_{2-x}Al$ give 1.5, 1.2, and 1.1, respectively.[40] With this, the combination of elevated temperature and similar mechanical properties of the higher order phases may help to mitigate the catastrophic degradation of cracks and pulverization, thus also enabling a longer electrode cycle life.

Asymmetrical Thermal Cycling of β-LiAl/Li_3Al_2/$Li_{2-x}Al$. With the primary motivation for this work stemming from the practical expectation that battery charging is likely to take place above room temperature, we must, by necessity, also consider the practical scenario of charging at elevated temperature but discharging at room temperature. More specifically, and as mentioned previously, it is known that the electrochemical formation of Li_3Al_2 and $Li_{2-x}Al$ necessitates elevated temperatures. However, the *delithiation* of

https://doi.org/10.1021/acsaem.2c03673
ACS Appl. Energy Mater. XXXX, XXX, XXX−XXX

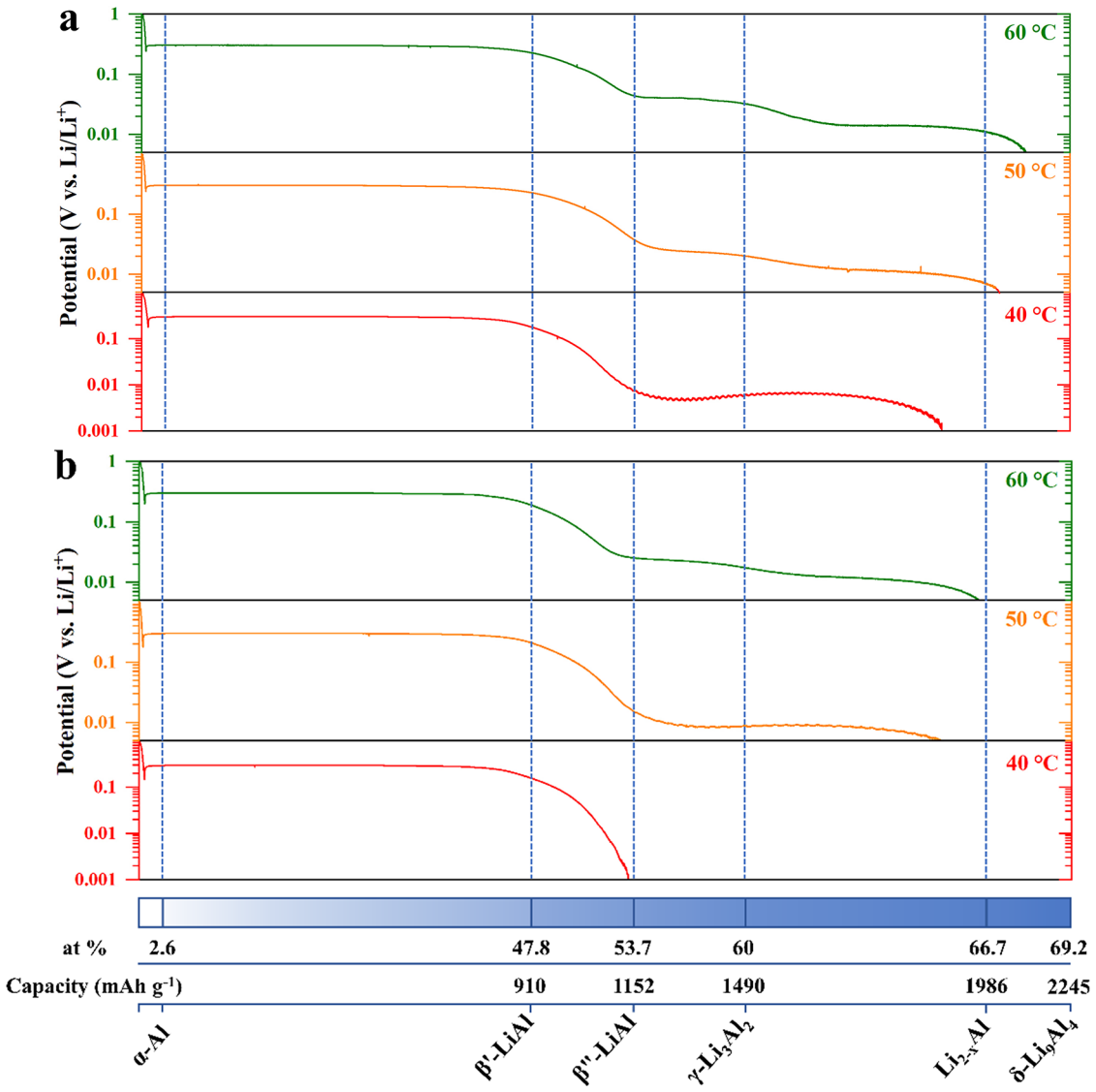

Figure 4. Electrochemical lithiation of Al thin film electrode at various temperatures within the moderate temperature regime. The lithiation current under galvanostatic mode is (a) 24 and (b) 48 μA cm^{-2}, which are equivalent to ∼C/20 and ∼C/10, respectively, normalized to the theoretical capacity of the β-LiAl.

those phases may not be under the same constraints, especially because a temperature as low as 35 °C is already sufficient to achieve the formation of Li_3Al_2 and $Li_{2-x}Al$, although at low rates.[29] Given the expectation of localized heating due to ohmic losses and Tafel kinetics, such temperatures may be realized at the nanoscale, even with room temperature ambient conditions.

With this in mind, we compare the GCD profiles of the two cells, both of which are lithiated at 60 °C, but one is delithiated at 60 °C (Figure 3a) and the other is delithiated at room temperature (Figure 3b). At 60 °C, the Al electrode functions the same as before with the three distinctive potential plateaus clearly observed. However, when the delithiation temperature is decreased to room temperature, plateaus **III*** and **II*** shift toward higher potential levels, generally consistent with the expectation that higher driving forces are required for removing Li from $Li_{2-x}Al$ and Li_3Al_2. Nevertheless, the overall charge efficiency is hardly affected by the RT delithiation. Also, quantitative data (Figure S4) are provided as additional support that the $Li_{2-x}Al/Li_3Al_2/\beta$-LiAl delithiation capacities are independent of temperature in this range. Regardless of the capacity variation between the cells, the ratios of the capacity by plateau **III*** + **II*** over the one by plateau **III** + **II** are almost the same, i.e., 114.3% at 60 °C vs 113.8% at RT, suggesting that the $Li_{2-x}Al/Li_3Al_2/\beta$-LiAl transformations give the same delithiation capacity level at both temperatures.

This asymmetrical thermal behavior and lithiation capability may be ideal for some applications, considering that the charging process of a full cell is equivalent to the lithiation of the anode. For EVs, as already mentioned, the heat accumulation during charging is not necessarily a negative thing, as it can warm up the battery pack in winter and facilitate a faster ion diffusion that positively affects the charging speed and reduces lithium plating risks. With an Al anode, the heat generated during the charge due to internal resistance may already be sufficient to facilitate the formation of Li_3Al_2 and $Li_{2-x}Al$ phases.

Rate and Temperature Dependence in Lithiation. The natural corollary to temperature if any charging scenario is to be considered would be that of charging rate (i.e., current

https://doi.org/10.1021/acsaem.2c03673
ACS Appl. Energy Mater. XXXX, XXX, XXX−XXX

density), given that efficiency loss and heat generation scale proportionally to this figure in any electrochemical system.

A systematic comparison of the galvanostatic lithiation profile of Al film electrodes at various temperatures with the lithiation current of 24 and 48 μA cm^{-2} is presented in Figure 4. In both cases, the specific capacities never reach the level equivalent to Li_9Al_4, even when accounting for electric charges contributed by surface reactions and/or electrolyte breakdown, indicating that the $Li_{2-x}Al$ phase is likely the highest lithiated phase in these cells.[29] At a slower lithiation rate (Figure 4a), the three plateaus (i.e., formation of β-LiAl, Li_3Al_2, and $Li_{2-x}Al$) discussed above can be observed at 60 and 50 °C with the y-axis in a logarithmic scale, suggesting that these phases are forming one after another. However, when the temperature is further decreased to 40 °C, the second (Li_3Al_2) and the third plateau ($Li_{2-x}Al$) seem to merge with each other, yielding a long plateau until reaching a specific capacity level that matches the $Li_{2-x}Al$ one. At 40 °C, when the Al film is transformed to the β-LiAl (i.e., >47.8 at % Li or >910 mAh g^{-1} Al), the lithiation potential drops to a level as low as ∼4 mV vs Li/Li$^+$ and slowly recovers to ∼7 mV vs Li/Li$^+$. This potential level is sufficiently low (i.e., <15 mV vs Li/Li$^+$) to facilitate the simultaneous formation of Li_3Al_2 and the $Li_{2-x}Al$. This experiment is also repeated at a higher lithiation current of 48 μA cm^{-2} (Figure 4b), and the results are then compared with the ones at 24 μA cm^{-2}. Although the galvanostatic profile at 60 °C almost maintains the same features, the potential plateaus of Li_3Al_2 and the $Li_{2-x}Al$ start merging at 50 °C rather than at 60 °C at this higher rate. Remarkably, the phases that are beyond β-LiAl can hardly form at 40 °C, and the lithiation stops within the β-LiAl composition, agreeing with Ghavidel et al. that a very slow lithiation rate is necessary to form those Li-rich phases at a similar temperature, e.g., 35 °C.[29] We also extracted all the quantitative data from Figure 4 and summarize them as Table S1 for easier comparisons. Although the comparisons imply slightly different kinetic behaviors among C-rates and temperatures, the electrode could work just fine at >50 °C for both rates and 40 °C for a lower rate.

Practical Implementation of Anodes with Higher-Order Phases. Because this study is the first to suggest cycling between the β-LiAl and the higher-order phases in the LIB cells that are expected to operate under ambient conditions, some practical implementation aspects should be acknowledged: Unlike conventional graphite anodes, β-LiAl itself serves as a Li reservoir (in the same way as the cathode), but prelithiation is essential to enabling this before final cell assembly. Various methods for lithiating Al (mechanical,[41,42] chemical,[43] and electrochemical[37]) have all been demonstrated to be effective for this purpose. Naturally, a prelithiated surface must be sufficiently stable (at least in a dry room), such that the fabrication process can be significantly simplified.[44] This would allow for not only the slurry-based mixing and baking processes to be abandoned, but a better understanding of prelithiated Al reactivity would allow for higher tolerance of the oxygen- and/or moisture-controlled conditions. For instance, reducing the grain size in Al foils via a shot-peening treatment before prelithiation is reported to be helpful to make a LiAl electrode stable in ambient air for several hours.[45] Alternatively, SEI engineering is also demonstrated to be beneficial to the β-LiAl, giving better air compatibility as well as a more stable cycling performance.[43,45,46]

The term "N-to-P ratio" (i.e., the capacity ratio of negative over positive electrode) is brought up to prevent Li plating from occurring on the surface of anodes. The possible short circuit induced by Li dendrites may lead to catastrophic incidents, e.g., explosions, fires, and so forth. Therefore, a typical value of the N-to-P ratio is ca. 1.1, indicating that the Li storage capability of the anode is slightly higher than that of the cathode. Interestingly, for β-LiAl, there exists a Li solubility range that contributes some capacity,[37] and this solubility range could potentially act as a buffer during charging when the temperature is insufficient for the formation of higher-order phases. Furthermore, the solid solution nature of the β-LiAl yields a linear relationship between the electrical potential and the Li content within this solubility range. Therefore, any unwanted risk of Li plating would likely be reflected by the cell voltage.

Lastly, the redox potentials for the lithiation−delithiation of Li_3Al_2 and $Li_{2-x}Al$ are ∼0.053 and ∼0.13 V vs Li/Li$^+$, respectively. These low potentials versus Li would give a higher voltage window in a full cell, and thus a higher energy density, as compared to those of β-LiAl (∼0.36 V), to those of other alloy anode candidates, such as silicon-based (0.2−0.6 V) and tin-based (0.2−1.2 V), and those of current state-of-the-art anodes, such as $Li_4Ti_5O_{12}$ (∼1.55 V) and graphite (0.1−0.2 V).[47] Importantly, the prestored Li in the β-LiAl also prevents the anode potential from varying too much (i.e., never beyond ∼0.42 V vs Li/Li$^+$), ensuring that the cell stays in the appropriate voltage window for power-sensitive applications. In short, although some practical considerations do exist, this study already demonstrates that cycling between β-LiAl and higher-order phases at slightly elevated temperatures has some advantages over α/β phase transformations. Of course, independent investigations are still required to explore the reliability and feasibility of this cycling strategy in practical applications.

SUMMARY AND RECOMMENDATIONS

To summarize, an alternative approach to utilizing Al alloy anodes is proposed in this study. Instead of the cycling between α-Al and β-LiAl, this work demonstrates the electrochemical reversibility among β-LiAl, Li_3Al_2, and $Li_{2-x}Al$ phases at slightly elevated temperatures. The cycling between β-LiAl and $Li_{2-x}Al$ yields a reversible capacity of ca. 950 mAh g^{-1}, normalized to the mass of Al. Conventional Al anode cells using the $\alpha \leftrightarrow \beta$ phase transformations completely lost their capacities both at room temperature and at 60 °C after a dozen cycles, while the cells utilizing β-LiAl ↔ $Li_{2-x}Al$ give a relatively stable performance with ca. 67% capacity retention after 100 cycles at 60 °C. Importantly, the lithiation−delithiation of β-LiAl/$Li_{2-x}Al$ exhibits thermally asymmetric features, i.e., only the β-LiAl to $Li_{2-x}Al$ phase transformations necessitate moderate temperatures. Evidence of long-term cycling improvements can be achieved via temperature and voltage control without altering any cell components or designs, thus offering a "plug-and-play" type of solution that is compatible with many application requirements.

Looking forward, the underlying mechanisms of the higher-order Li−Al phases are poorly understood compared to β-LiAl, requiring further investigations in systematic ways. New studies into the lithiation kinetics may reveal the whole picture of the lithiation−delithiation processes of the Li−Al electrochemical system, particularly with overpotentials being linked at various rates and temperatures. Moreover, the mechanical properties are attractive to investigate as the better cycling performance may benefit from the similar mechanical properties of β-LiAl/

https://doi.org/10.1021/acsaem.2c03673
ACS Appl. Energy Mater. XXXX, XXX, XXX−XXX

$Li_3Al_2/Li_{2-x}Al$. Certainly, other aspects of the material such as surface activities and structures can also be of vital importance as interfaces and interphases are well-known to be key enablers of LIB technology. *In situ* or *operando* SEM and XRD techniques can be very helpful due to the high reactivity of Li–Al intermetallic compounds.

■ ASSOCIATED CONTENT

Supporting Information

The Supporting Information is available free of charge at https://pubs.acs.org/doi/10.1021/acsaem.2c03673.

Cyclic voltammograms of Al thin film electrodes; galvanostatic charge–discharge (GCD) profiles of an LTO–Al thin film full cell at 60 °C; GCD profiles of α/β phase transformations in half-cells at 60 °C and room temperature; analyses of delithiation capacities at 60 °C and room temperature; electrochemical parameters extracted from the GCD profiles at various temperatures (PDF)

■ AUTHOR INFORMATION

Corresponding Authors

Tianye Zheng − *Department of Electrical Engineering and Photonics Research Institute, The Hong Kong Polytechnic University, Hung Hom, Kowloon 999077, Hong Kong;* orcid.org/0000-0002-2281-9506; Email: darren.ty.zheng@connect.polyu.hk

Steven T. Boles − *Department of Energy and Process Engineering, Norwegian University of Science and Technology, 7491 Trondheim, Norway;* orcid.org/0000-0003-1422-5529; Email: steven.boles@ntnu.no

Authors

Jia Zhang − *Department of Electrical Engineering, The Hong Kong Polytechnic University, Hung Hom, Kowloon 999077, Hong Kong*

Wei Jin − *Department of Electrical Engineering and Photonics Research Institute, The Hong Kong Polytechnic University, Hung Hom, Kowloon 999077, Hong Kong*

Complete contact information is available at: https://pubs.acs.org/10.1021/acsaem.2c03673

Notes

The authors declare no competing financial interest.

■ ACKNOWLEDGMENTS

T.Z. acknowledges the "PolyU Distinguished Postdoctoral Fellowship Scheme" (1-YWBT) at The Hong Kong Polytechnic University (PolyU). S.T.B. acknowledges the ENERSENSE research initiative (68024013) at Norwegian University of Science and Technology (NTNU), Norway. The authors are thankful to Dr. Dominik Kramer and Dr. Reiner Mönig from the IAM-MMI of Karlsruhe Institute of Technology (KIT), Germany, for the technical discussion.

■ REFERENCES

(1) Flandrois, S.; Simon, B. Carbon materials for lithium-ion rechargeable batteries. *Carbon* **1999**, *37* (2), 165–180.

(2) Whittingham, M. S. History, Evolution, and Future Status of Energy Storage. *Proc. IEEE* **2012**, *100*, 1518–1534.

(3) Chianelli, R. R. Microscopic studies of transition metal chalcogenides. *J. Cryst. Growth* **1976**, *34* (2), 239–244.

(4) Rao, B.; Francis, R.; Christopher, H. Microscopic studies of transition metal chalcogenides. *J. Electrochem. Soc.* **1977**, *124* (10), 1490–1492.

(5) Yao, N.; Heredy, L.; Saunders, R. J. Lithium - aluminum electrode. *J. Electrochem. Soc.* **1971**, *118* (7), 1039–1042.

(6) Melendres, C. A. Kinetics of electrochemical incorporation of lithium into aluminum. *J. Electrochem. Soc.* **1977**, *124* (5), 650–655.

(7) Besenhard, J. O. Cycling behaviour and corrosion of Li-Al electrodes in organic electrolytes. *J. Electroanal. Chem.* **1978**, *94* (1), 77–81.

(8) Kishio, K.; Brittain, J. O. Defect structure of β-LiAl. *J. Phys. Chem. Solids* **1979**, *40* (12), 933–940.

(9) Wen, C. J.; Boukamp, B. A.; Huggins, R. A.; Weppner, W. Thermodynamic and mass transport properties of "LiAl. *J. Electrochem. Soc.* **1979**, *126* (12), 2258–2266.

(10) Wen, C. J.; Weppner, W.; Boukamp, B. A.; Huggins, R. A. Electrochemical investigtion of solubility and chemical diffusion of lithium in aluminum. *Metall. Trans B* **1980**, *11* (1), 131–137.

(11) Frazer, E. J. Electrochemical formation of lithium-aluminium alloys in propylene carbonate electrolytes. *J. Electroanal. Chem.* **1981**, *121*, 329–339.

(12) Noble, B.; Harris, S. J.; Dinsdale, K. The elastic modulus of aluminium-lithium alloys. *J. Mater. Sci.* **1982**, *17* (2), 461–468.

(13) Baranski, A.; Fawcett, W. The Formation of Lithium-Aluminum Alloys at an Aluminum Electrode in Propylene Carbonate. *J. Electrochem. Soc.* **1982**, *129* (5), 901–907.

(14) Jow, T.; Liang, C. Lithium - Aluminum Electrodes at Ambient Temperatures. *J. Electrochem. Soc.* **1982**, *129* (7), 1429–1434.

(15) Geronov, Y.; Zlatilova, P.; Moshtev, R. V. The secondary lithium-aluminium electrode at room temperature: I. Cycling in $LiClO_4$-propylene carbonate solutions. *J. Power Sources* **1984**, *12* (2), 145–153.

(16) Geronov, Y.; Zlatilova, P.; Staikov, G. The secondary lithium-aluminium electrode at room temperature: II. Kinetics of the electrochemical formation of the lithium-aluminium alloy. *J. Power Sources* **1984**, *12* (2), 155–165.

(17) Geronov, Y.; Zlatilova, P.; Staikov, G. Electrochemical nucleation and growth of β-LiAl alloy in aprotic electrolyte solutions. *Electrochim. Acta* **1984**, *29* (4), 551–555.

(18) Maskell, W.; Owen, J. Cycling behavior of thin film LiAl electrodes with liquid and solid electrolytes. *J. Electrochem. Soc.* **1985**, *132* (7), 1602–1607.

(19) Yoshino, A. The Birth of the Lithium-Ion Battery. *Angew. Chem., Int. Ed.* **2012**, *51* (24), 5798–5800.

(20) Hudak, N. S.; Huber, D. L. Nanostructured lithium-aluminum alloy electrodes for lithium-ion batteries. *ECS Trans.* **2011**, *33* (24), 1–13.

(21) Hudak, N. S.; Huber, D. L. Size effects in the electrochemical alloying and cycling of electrodeposited aluminum with lithium. *J. Electrochem. Soc.* **2012**, *159* (5), A688–A695.

(22) Chan, A. K.; Tatara, R.; Feng, S.; Karayaylali, P.; Lopez, J.; Stephens, I. E.; Shao-Horn, Y. *J. Electrochem. Soc.* **2019**, *166* (10), A1867–A1874.

(23) Tahmasebi, M. H.; Kramer, D.; Mönig, R.; Boles, S. T. Insights into Phase Transformations and Degradation Mechanisms in Aluminum Anodes for Lithium-Ion Batteries. *J. Electrochem. Soc.* **2019**, *166* (3), A5001–A5007.

(24) Abe, I.; Horiba, T.; Abe, Y.; Hida, K.; Matsuyama, T.; Yasuno, S.; Komaba, S. Investigation and Improvement of Metallic Aluminum as Alloying Electrode in Non-Aqueous Li Cells. *J. Electrochem. Soc.* **2020**, *167* (11), 110513.

(25) Chang, X.; Xie, Z.; Liu, Z.; Zheng, X.; Zheng, J.; Li, X. Aluminum: An underappreciated anode material for lithium-ion batteries. *Energy Storage Mater.* **2020**, *25*, 93–99.

(26) Wang, H.; Tan, H.; Luo, X.; Wang, H.; Ma, T.; Lv, M.; Song, X.; Jin, S.; Chang, X.; Li, X. The progress on aluminum-based anode materials for lithium-ion batteries. *J. Mater. Chem. A* **2020**, *8* (48), 25649–25662.

(27) Qin, B.; Diemant, T.; Zhang, H.; Hoefling, A.; Behm, R. J.; Tübke, J.; Varzi, A.; Passerini, S. *ChemSusChem* **2019**, *12* (12), 2609−2619.
(28) Puhakainen, K.; Boström, M.; Groy, T. L.; Häussermann, U. A new phase in the system lithium−aluminum: Characterization of orthorhombic Li_2Al. *J. Solid State Chem.* **2010**, *183* (11), 2528−2533.
(29) Ghavidel, M. Z.; Kupsta, M. R.; Le, J.; Feygin, E.; Espitia, A.; Fleischauer, M. D. *J. Electrochem. Soc.* **2019**, *166* (16), A4034−A4040.
(30) Lithium Ion Batteries (Li-Ion), Panasonic Corporation of North America, 2022; https://na.industrial.panasonic.com/products/batteries/rechargeable-batteries/lineup/lithium-ion (accessed 2022-11-15).
(31) McAlister, A. J. The Al−Li (Aluminum−Lithium) system. *Bull. Alloy Phase Diagrams* **1982**, *3*, 177−183.
(32) Murray, J. L.; Bennett, L. H.; Baker, H.*Binary Alloy Phase Diagrams*; American Society for Metals: OH, 1986; Vol. *1*.
(33) Zheng, T.; Wang, X.; Jain, E.; Kramer, D.; Monig, R.; Seita, M.; Boles, S. T. Granular phase transformation of polycrystalline aluminum during electrochemical lithiation. *Scr. Mater.* **2020**, *188*, 164−168.
(34) Zheng, T.; Kramer, D.; Tahmasebi, M. H.; Mönig, R.; Boles, S. T. Improvement of the Cycling Performance of Aluminum Anodes through Operando Light Microscopy and Kinetic Analysis. *ChemSusChem* **2020**, *13* (5), 974−985.
(35) Zheng, T.; Kramer, D.; Tahmasebi, M. H.; Mönig, R.; Boles, S. T. Exploring the Reversibility of Phase Transformations in Aluminum Anodes through Operando Light Microscopy and Stress Analysis. *ChemSusChem* **2020**, *13* (22), 5910−5920.
(36) Li, H.; Yamaguchi, T.; Matsumoto, S.; Hoshikawa, H.; Kumagai, T.; Okamoto, N. L.; Ichitsubo, T. Circumventing huge volume strain in alloy anodes of lithium batteries. *Nat. Commun.* **2020**, *11* (1), 1584.
(37) Zheng, T.; Kramer, D.; Mönig, R.; Boles, S. T. Aluminum Foil Anodes for Li-Ion Rechargeable Batteries: the Role of Li Solubility within β-LiAl. *ACS Sustain. Chem. Eng.* **2022**, *10* (10), 3203−3210.
(38) Huang, T. S.; Brittain, J. O. The mechanical behavior of β-LiAl. *Mater. Sci. Eng.* **1987**, *93*, 93−97.
(39) Liu, Y.; Hudak, N. S.; Huber, D. L.; Limmer, S. J.; Sullivan, J. P.; Huang, J. Y. In Situ Transmission Electron Microscopy Observation of Pulverization of Aluminum Nanowires and Evolution of the Thin Surface Al2O3 Layers during Lithiation−Delithiation Cycles. *Nano Lett.* **2011**, *11* (10), 4188−4194.
(40) Sarmiento-Pérez, R.; Cerqueira, T. F. T.; Valencia-Jaime, I.; Amsler, M.; Goedecker, S.; Romero, A. H.; Botti, S.; Marques, M. A. L. Novel phases of lithium-aluminum binaries from first-principles structural search. *J. Chem. Phys.* **2015**, *142* (2), 024710.
(41) Ryu, J.; Kang, J.; Kim, H.; Lee, J. H.; Lee, H.; Park, S. Electrolyte-mediated nanograin intermetallic formation enables superionic conduction and electrode stability in rechargeable batteries. *Energy Storage Mater.* **2020**, *33*, 164−172.
(42) Yu, Y.; Li, S.; Fan, H.; Xu, H.; Jiang, M.; Huang, Y.; Li, J. Optimal annealing of Al foil anode for prelithiation and full-cell cycling in Li-ion battery: The role of grain boundaries in lithiation/delithiation ductility. *Nano Energy* **2020**, *67*, 104274.
(43) Huang, Y.; Liu, C.; Wei, F.; Wang, G.; Xiao, L.; Lu, J.; Zhuang, L. Chemical prelithiation of Al for use as an ambient air compatible and polysulfide resistant anode for Li-ion/S batteries. *J. Mater. Chem. A* **2020**, *8*, 18715−18720.
(44) Zheng, T.; Boles, S. T. Simplifying Electrode Design for Lithium-Ion Rechargeable Cells. *ACS Omega* **2022**, *7* (42), 37867−37872.
(45) Fan, H.; Li, S.; Yu, Y.; Xu, H.; Jiang, M.; Huang, Y.; Li, J. Air-Stable Li_xAl Foil as Free-Standing Electrode with Improved Electrochemical Ductility by Shot-Peening Treatment. *Adv. Funct. Mater.* **2021**, *31*, 2100978.
(46) Heligman, B. T.; Manthiram, A. Elemental Foil Anodes for Lithium-Ion Batteries. *ACS Energy Lett.* **2021**, *6*, 2666−2672.
(47) Eftekhari, A. Low voltage anode materials for lithium-ion batteries. *Energy Storage Mater.* **2017**, *7*, 157−180.

https://doi.org/10.1021/acsaem.2c03673
ACS Appl. Energy Mater. XXXX, XXX, XXX−XXX